

## Solid-state screening effect on the post-collision interaction

T. Miller and T.-C. Chiang

*Department of Physics and Materials Research Laboratory, University of Illinois at Urbana-Champaign, Urbana, Illinois 61801*

(Received 11 October 1983)

Photoexcited  $N_{4,5}O_{1,2,3}$  Auger transitions for  $\text{La}^{3+}$  in  $\text{LaF}_3$ , an insulator, are studied with the photon energy tuned through the  $\text{La } 4d$  to  $4f$  resonant excitations. The post-collision interaction between the photoexcited electron and the Auger electron leads to a shift in the Auger kinetic energies. The shift is reduced by 2.3 eV for the same Auger transitions in  $\text{LaB}_6$ , a metal, due to metallic screening.

Photoexcited Auger events in an atom are usually described as a process involving two independent steps: The removal of a core electron from the atom by photoemission and the subsequent Auger decay of the core hole. This description is quite accurate if the incident photon energy is much higher than the core photothreshold for continuum excitation; in this case the photoelectron is promptly removed from the atom and is decoupled from the slower Auger event. However, for excitations barely above threshold, the Coulomb repulsion between the slowly receding photoelectron and the Auger electron can produce an upward shift of the Auger electron kinetic energy. For excitations to bound states below threshold, the exchange and correlation energies can also be significant in addition to the Coulomb interaction. The measured shifts can be as large as a few electron volts. The interaction between the photoexcited electron and the Auger electron, known as the post-collision interaction (PCI),<sup>1-4</sup> has attracted much attention recently because it provides a means to probe the nature of the photoexcited states and the Auger decay processes.

If the photoexcited Auger process occurs in a solid-state environment, screening of the charges can substantially modify the PCI shifts. Although much work on PCI has been done in solids,<sup>2,4</sup> the screening effect has not been investigated thoroughly. In a metal, all charges are screened in a very short distance on the order of an atomic radius in the adiabatic limit, thus the long-range Coulomb interaction between charges is reduced.<sup>5</sup> Considering the same Auger process in a wide-gap insulator for which screening is merely the long-range dielectric polarization, the PCI shift due to the Coulomb interaction can be much larger than in a metal. In this paper, we report the first observation of this effect. We measured the PCI shift for the  $N_{4,5}O_{1,2,3}$  Auger transitions of  $\text{La}^{3+}$  in  $\text{LaF}_3$ , an insulator, and found a much larger Coulomb shift compared with the same transitions in  $\text{LaB}_6$ , a metal.

The experiment was done at the Synchrotron Radiation Center at Stoughton, Wisconsin. A 3-m toroidal-grating monochromator and a double cylindrical-mirror analyzer were used to acquire the photoemission and Auger spectra. The  $\text{LaF}_3$  samples were prepared by evaporating a thin layer (about 200 Å thick) onto a tungsten foil at room temperature. There was no measurable charging effect for these thin layers.

Figure 1 shows a partial-yield spectrum for  $\text{LaF}_3$  obtained by measuring the secondary-electron current with kinetic energy  $5.9 \pm 0.2$  eV while scanning the incident photon en-

ergy. The three peaks *a*, *c*, and *e* correspond to quasiatomic transitions for  $\text{La}^{3+}$  from the ground state  $4d^{10} ({}^1S_0)$  to the excited states  $4d^9 4f^1 ({}^3P_1, {}^2D_1, \text{ and } {}^1P_1)$ , respectively. The two lower transitions (peaks *a* and *c*) are below threshold for continuum excitation (promoting a  $4d$  electron to the conduction band), and therefore are very sharp. The higher transition (peak *e*) is above threshold and is broadened. These transitions have been studied quite extensively before.<sup>6,7</sup>

Some typical photoemission spectra are shown in Fig. 2. The photon energies used for spectra *a-g* are 97.08, 99.00, 101.53, 114.87, 116.87, 120.87, and 128.87 eV, respectively; they are indicated by arrows *a-g* in Fig. 1. In Fig. 2 the valence band (mainly  $\text{F } 2p$ ) as well as  $\text{La } 5p$  (two components due to spin-orbit splitting),  $\text{F } 2s$ , and  $\text{La } 5s$  core levels can be clearly seen; these are labeled for spectrum *g*. The measured binding energies ( $\pm 0.1$  eV) for various states relative to the Fermi level are 9.7 (peak of the valence band), 20.8, ( $\text{La } 5p_{3/2}$ ), 23.4 ( $\text{La } 5p_{1/2}$ ), 31.3 ( $\text{F } 2s$ ), 38.6 ( $\text{La } 5s$ ), 106.6 ( $\text{La } 4d_{5/2}$ ), and 109.6 eV ( $\text{La } 4d_{3/2}$ ), respectively. The two broad features labeled *A* and *B* for spectrum *g* in Fig. 2 originate from quasiatomic  $\text{La}$ -derived  $N_{4,5}O_{1,2,3}$  and  $N_{4,5}O_{2,3}O_{2,3}$  Auger transitions, respectively. This assignment is based on comparison with known Auger spectra of isoelectronic  $\text{I}^-$ ,  $\text{Xe}$ , and  $\text{Cs}^+$ .<sup>4,8</sup>

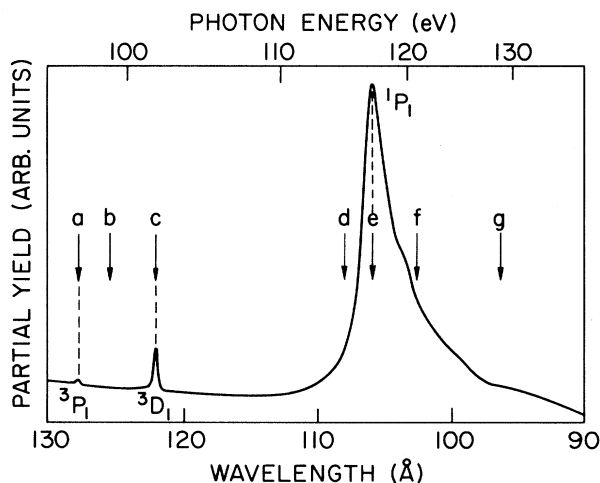


FIG. 1. Partial-yield spectrum for  $\text{LaF}_3$ . The arrows *a-g* indicate photon energies used to obtain spectra *a-g* in Fig. 2, respectively.

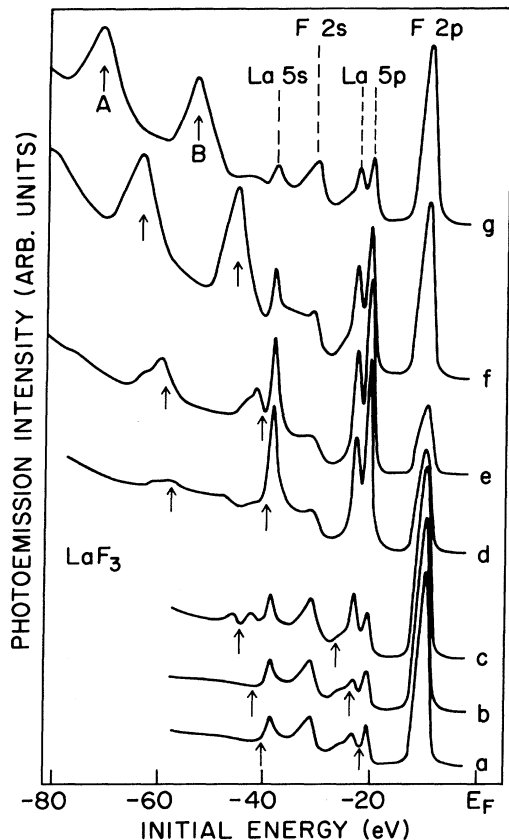
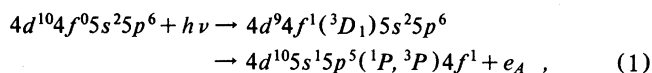


FIG. 2. Photoemission spectra for  $\text{LaF}_3$ . Spectra *a*–*g* are taken with photon energies indicated by arrows *a*–*g* in Fig. 1, respectively. The initial-energy scale is referenced to the Fermi level ( $E_F$ ) of the metal substrate. The two arrows indicate positions of constant kinetic energies.

From the measured core-level binding energies, the effective Coulomb interaction between the two holes in the Auger final state is roughly 15 eV.<sup>9</sup> These transitions were also observed in  $\text{LaB}_6$  with comparable intensities. The previous assignment<sup>7</sup> that the features *A* and *B* were derived from  $\text{La-N}_{4,5}\text{O}_1V$  and  $\text{N}_{4,5}\text{O}_{2,3}V$  Auger transitions (*V* stands for the valence orbitals) could not be correct, because  $\text{LaF}_3$ , being ionic, should show negligible *NOV* Auger intensities compared with  $\text{LaB}_6$ . The two arrows in Fig. 2 indicate positions of constant kinetic energies; the two Auger features show dramatic changes in intensity and line shape as the photon energy is tuned through the absorption features shown in Fig. 1.<sup>10</sup> Here we will focus attention on the energies of  $\text{N}_{4,5}\text{O}_{1,2,3}$  Auger transitions, feature *A* in Fig. 2. Feature *B* overlaps often with strong photoemission lines, and its analysis is more difficult.

Auger feature *A* is plotted versus the kinetic energy in Fig. 3 as a function of photon energy  $h\nu$  with an expanded scale to show details. For  $h\nu = 101.53$  eV (position *c* in Fig. 1), two sharp peaks corresponding to the  $^1P$  and  $^3P$  Auger final states are observed.<sup>8</sup> The transitions are



where  $e_A$  denotes the Auger electron. The splitting within

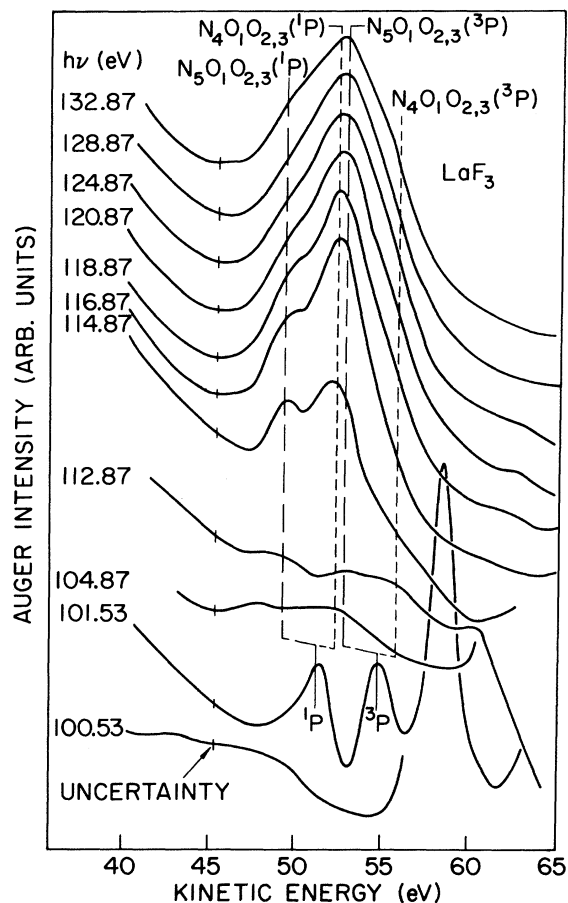
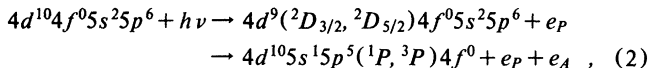


FIG. 3.  $\text{N}_{4,5}\text{O}_{1,2,3}$  Auger spectra for  $\text{LaF}_3$ . The bars labeled “uncertainty” represent noise level in the original spectra before smoothing. The energy resolution is 0.3 eV. The excitation photon energies ( $h\nu$ ) are indicated.

the  $^1P$  and  $^3P$  manifolds due to coupling to the  $4f$  electron, spin-orbit coupling, and crystal-field effect is small and not resolved. The strong peak in Fig. 3 for  $h\nu = 101.53$  eV is the  $\text{La } 5s$  photoemission peak. For  $h\nu = 100.53, 104.87,$  and  $112.87$  eV, the Auger intensity is essentially zero, because the absorption (Fig. 1) is very small; the background variation is due to some unidentified loss features associated with photoemission peaks. For  $h\nu \geq 114.87$  eV in Fig. 3, continuum states far above threshold are reached, and the excitation and Auger decay processes are essentially decoupled. The transitions are



where  $e_P$  denotes the photoelectron. The spectrum thus consists of four peaks, i.e., each of the two photoexcited states ( $^2D_{3/2}$  and  $^2D_{5/2}$ ) gives rise to two Auger peaks  $^1P$  and  $^3P$ . The positions of these peaks are indicated by long- and short-dashed lines for the initial  $^2D_{5/2}$  and  $^2D_{3/2}$  states, respectively, in Fig. 3. The  $^1P$  and  $^3P$  splitting is obtained from the spectrum with  $h\nu = 101.53$  eV, and the  $^2D_{5/2}$ – $^2D_{3/2}$  splitting is obtained from photoemission (spectrum not shown). The change in line shape seen in Fig. 3 as  $h\nu$  increases from 114.87 to 132.87 eV is mainly due to drastic

changes in the  ${}^2D_{5/2}$ - ${}^2D_{3/2}$  photoemission branching ratio in this energy range: the  ${}^2D_{5/2}$  channel predominates at the lower-energy end, and both the  ${}^2D_{5/2}$  and  ${}^2D_{3/2}$  channels are about equal in intensity at higher energies.<sup>10</sup> Since the background function including some overlapping direct photoemission features is uncertain, we do not attempt to deconvolve the spectra. The above analysis, however, does explain the spectra qualitatively. From the relative Auger energies for processes described by Eqs. (1) and (2), one can show easily that the binding energy of the  $4f^1$  electron for the state  $4d^{10}5s5p^5({}^3P, {}^1P)4f^1$  relative to the Fermi level is 6.9 eV.

The same La-derived atomiclike Auger transitions in  $\text{LaB}_6$  have been observed and reported before.<sup>7,11</sup> For excitations far above threshold (e.g.,  $h\nu = 114.87\text{--}132.87$  eV for  $\text{LaF}_3$  in Fig. 3), the Auger transitions are essentially free from PCI, and the difference between Auger energies from  $\text{LaF}_3$  and  $\text{LaB}_6$  is due to differences in work functions, crystal (Madelung) potentials, relaxation energies, etc. For a measure of the PCI shift, consider the quantity  $\Delta E$  which is the difference between the kinetic energy of the  ${}^1P$  Auger line for resonant excitation into the  ${}^3D_1$  absorption line below threshold (peak *c* in Fig. 1) and the kinetic energy of the  $N_5O_1O_{2,3}$  ( ${}^1P$ ) Auger line for excitation far above threshold.  $\Delta E = 1.8$  eV for  $\text{LaF}_3$  from Fig. 3 and  $\Delta E \approx -0.5$  eV for  $\text{LaB}_6$  from data presented in Ref. 7. The difference between these two values for  $\Delta E$ , about 2.3 eV, reflects mainly the difference in solid-state screening (final-state effect) between  $\text{LaF}_3$  and  $\text{LaB}_6$ . We show below that the initial-state effect is much smaller. Denoting the effective Coulomb energy between the  $5s$  and  $5p$  core holes in the Auger final state by  $U(5s5p)$ , the Auger kinetic energy for excitations far above threshold is given by<sup>9</sup>

$$E(A) = E(4d) - E(5s) - E(5p) - U(5s5p) , \quad (3)$$

where  $E(4d)$  is the single-particle binding energy of the  $4d$  state, etc. For resonant excitations, the Auger energy is

$$E_R(A) = E(4d \rightarrow 4f) - E(5s) - E(5p) + E(4f) - U(5s5p\overline{4f}) , \quad (4)$$

where the first term is the  $4d$  to  $4f$  excitation energy, the next three terms give the single-particle binding energies for the  $5s$ ,  $5p$ , and  $4f$  levels, respectively, and the last term represents the effective interaction among the  $4f$  electron and the  $5s$  and  $5p$  holes. We also have

$$E(4d \rightarrow 4f) = E(4d) - E(4f) - U(4d\overline{4f}) , \quad (5)$$

where  $U(4d\overline{4f})$  is the effective energy between the  $4d$  hole and the  $4f$  electron. Combining Eqs. (3), (4), and (5), we obtain

$$\begin{aligned} \Delta E &= E_R(A) - E(A) \\ &= U(5s5p) - U(5s5p\overline{4f}) - U(4d\overline{4f}) . \end{aligned} \quad (6)$$

The first two terms on the right-hand side reflect the final-state effect. The last term in Eq. (6), reflecting the initial-state effect, is essentially independent of the solid-state environments, because the  $4d^9 4f^1({}^3D_1)$  state is spatially compact, and the valence electrons are insensitive to the  $4d$  to  $4f$  inner-shell transitions. It has been observed that the  ${}^3D_1$  excitation energies for La vary only by about 0.1 eV in different solid-state environments.<sup>6,12</sup> Therefore the difference in  $\Delta E$ , about 2.3 eV, is indeed dominated by the final-state effect. We emphasize that the above argument generally cannot be applied to other systems, e.g., those involving  $p$  to  $d$  transitions,<sup>13</sup> for which the initial-state effect is generally not negligible.

In summary, PCI shifts are influenced by solid-state screening effects. Comparing an insulator,  $\text{LaF}_3$ , with a metal,  $\text{LaB}_6$ , the PCI shift in  $\text{LaF}_3$  is larger by about 2.3 eV. This is due to metallic screening in  $\text{LaB}_6$ , which suppresses the Coulomb repulsion between the photoexcited electron and the Auger electron. The Coulomb repulsion contributes typically a few electron volts to the PCI shifts for excitations to bound states; therefore the observed difference in PCI shifts is of the correct order of magnitude. A detailed calculation of this screening effect with realistic wave functions and decay rates is not yet available. The final state of the Auger transition for La in  $\text{LaB}_6$  is probably  $4d^{10}5s^{15}p^5({}^1P, {}^3P)4f^1V^1$  independent of excitation conditions, where  $V$  is a  $5d$  or  $6s$  valence orbital. Assuming metallic screening in  $\text{LaB}_6$  proceeds infinitely fast, the following simple picture applies. For excitation to a bound state, the photoexcited electron occupies a screening level; for excitation to a high-lying continuum state, the photoelectron leaves fast, but the atom remains neutral by pulling an electron from the conduction band into the screening level. The Auger electron experiences the same interaction with the La atom independent of the excitation process; therefore the PCI shift is suppressed.

#### ACKNOWLEDGMENTS

This research was partially supported by the U.S. Department of Energy, Division of Materials Sciences, under Contract No. DE-AC02-76ER01198. Some of the equipment used for this research was obtained with grants from the Research Corporation and the General Motors Research Laboratories. We are grateful to E. W. Plummer for the use of his monochromator, to F. C. Brown and his group for help on computer programming and interfacing, and to E. Rowe and the staff of the Synchrotron Radiation Center for assistance. The Synchrotron Radiation Center is supported by the NSF under Contract No. DMR-80-20164.

<sup>1</sup>V. Schmidt, in *X-Ray and Atomic Inner-Shell Physics—1982*, edited by B. Crasemann, AIP Conf. Proc. No. 94 (AIP, New York, 1982), pp. 544–558, and references therein.

<sup>2</sup>M. K. Bahl, R. L. Watson, and K. J. Irgolic, Phys. Rev. Lett. **42**, 165 (1979).

<sup>3</sup>W. Eberhardt, G. Kalkoffen, and C. Kunz, Phys. Rev. Lett. **41**, 156 (1978).

<sup>4</sup>T.-C. Chiang, D. E. Eastman, F. J. Himpsel, G. Kaindl, and M. Aono, Phys. Rev. Lett. **45**, 1846 (1980).

<sup>5</sup>J. W. Gadzuk, in *Photoemission and the Electronic Properties of Surfaces*, edited by B. Feuerbacher, B. Fitton, and R. F. Willis (Wiley, New York, 1978), pp. 111–136.

<sup>6</sup>S. Suzuki, T. Ishii, and T. Sagawa, J. Phys. Soc. Jpn. **38**, 156 (1975).

<sup>7</sup>M. Aono, T.-C. Chiang, J. A. Knapp, T. Tanaka, and D. E. Eastman, *Phys. Rev. B* 21, 2661 (1980).

<sup>8</sup>L. O. Werme, T. Bergmark, and K. Siegbahn, *Phys. Scr.* 6, 141 (1972).

<sup>9</sup>E. Antonides, E. C. Janse, and G. A. Sawatzky, *Phys. Rev. B* 15, 1669 (1977).

<sup>10</sup>M. Aono, T.-C. Chiang, F. J. Himpsel, and D. E. Eastman, *Solid State Commun.* 37, 471 (1981).

<sup>11</sup>The analysis in Ref. 7 was not entirely correct due to misassign-

ment of the Auger transitions.

<sup>12</sup>Different authors give different values for the transition energies due to miscalibration of the monochromators. The data presented in Ref. 6 were obtained using one monochromator; the measured differences in transition energies must be reliable.

<sup>13</sup>M. R. Thuler, R. L. Benbow, and Z. Hurych, *Phys. Rev. B* 27, 2082 (1983); T.-C. Chiang and D. E. Eastman, *ibid.* 21, 5749 (1980).